

# The winking eye of a hefty star. WR 21a revealed as a very massive eclipsing binary by *TESS*

Rodolfo H. Barbá<sup>1\*</sup>, Roberto C. Gamen<sup>2,3</sup>, Pablo Martín-Ravelo<sup>1</sup>, Julia I. Arias<sup>1</sup>, and Nidia I. Morrell<sup>4</sup>

<sup>1</sup>Departamento de Astronomía, Universidad de La Serena, Av. Cisternas 1200 Norte, La Serena, Chile.

<sup>2</sup>Instituto de Astrofísica de La Plata, CONICET–UNLP, Paseo del Bosque s/n, La Plata, Argentina.

<sup>3</sup>Facultad de Ciencias Astronómicas y Geofísicas, Universidad Nacional de La Plata, Argentina.

<sup>4</sup>Las Campanas Observatory, Carnegie Observatories, Casilla 601, La Serena, Chile.

Accepted XXX. Received YYY; in original form ZZZ

## ABSTRACT

WR 21a was known as a massive spectroscopic binary composed of an O2.5 If\*/WN6ha primary and an O3 V((f\*))z secondary. Although a minimum value, the mass estimated for the primary placed it as one of the most massive stars found in our Galaxy. We report the discovery of photometric variations in the time series observations carried out by the Transiting Exoplanet Survey Satellite (*TESS*). These light variations are interpreted as formed by two main components: a sharp partial eclipse of the O3 by the O2.5/WN6 star, and tidally excited oscillations. Based on the light minima a new ephemeris for the system is calculated. The system configuration is detached and the observed eclipse corresponds to the periastron passage. During the eclipse, the light curve shape suggests the presence of the *heartbeat effect*. The frequencies derived for the tidally excited oscillations are harmonics of the orbital period. Combining new and previously published radial velocity measurements, a new spectroscopic orbital solution is also obtained. Using the *PHOEBE* code we model the *TESS* light curve and determine stellar radii of  $R_{\text{O2.5/WN6}} = 23.3 R_{\odot}$  and  $R_{\text{O3}} = 14.8 R_{\odot}$  and an orbital inclination  $i = 61^{\circ}8 \pm 1^{\circ}5$ . The latter combined with the spectroscopic minimum masses lead to absolute masses of  $M_{\text{O2.5/WN6}} = 94.4 M_{\odot}$  and  $M_{\text{O3}} = 53.6 M_{\odot}$ , which establishes WR 21a as belonging to the rare group of the very massive stars.

**Key words:** binaries: close – stars: massive – stars: fundamental parameters – stars: oscillations – stars: Wolf–Rayet – stars: individual: WR 21a

## 1 INTRODUCTION

Although few in the Galaxy, massive stars are key astrophysical objects in view of the influence they exert on their environment. Among them, very massive stars (VMS), i.e. those with masses above  $M \gtrsim 60 M_{\odot}$  (Langer 2012), form a special group. These rare and extreme objects defy the current scenarios of massive star formation, evolution and stellar death (Vink 2015). Few specimens of the VMS class exist in the Local Group, being all concentrated in massive young clusters. Famous examples are the members of R136 at the 30 Doradus starburst in the Large Magellanic Cloud (Crowther et al. 2010) and NGC 3603-A1 in our Galaxy (Schnurr et al. 2008). VMS are representative of the top end of the initial mass function. The masses of VMS are generally estimated using stellar atmosphere and radiative transfer codes (e.g. Bestenlehner et al. 2020, for R136a1, R136a2, and R136a3), or empirically determined from the simultaneous spectroscopic and photometric analysis of eclipsing binary systems (e.g. Bonanos et al. 2004, for WR 20a). Apart from the few existing astrometric binary systems, eclipsing binaries provide the most reliable determinations of absolute stellar masses, as well as other important parameters such as stellar radii, surface gravities, etc.

Massive stars tend to live in binary or multiple systems (Sana

et al. 2012; Sana 2017; Barbá et al. 2017), most of them composing short-period binaries. During the last years, high-cadence space imaging surveys are revolutionising the time-domain Astrophysics and, specially, the realm of the massive stars. The *Transiting Exoplanet Survey Satellite* (*TESS*; Ricker et al. 2015) is a breakthrough example of such revolution. *TESS* has revealed hundreds of new massive eclipsing and ellipsoidal binary systems (e.g. Bursens et al. 2020; Trigueros Páez et al. 2021), opening the possibility of having a huge set of systems suitable for the calculation of precise stellar masses.

WR 21a (=THA 35-II-42, CDS 2134) was first identified as an H $\alpha$  emission star near the Carina Nebula region (The 1966; Wackerling 1970). It was detected as an X-ray source (=1E 1024.0-5732) with the *Einstein* satellite (Caraveo et al. 1989), subsequently identified as a Wolf-Rayet (WR) star (Mereghetti et al. 1994), and added to the *Catalogue of Galactic Wolf-Rayet Stars* (van der Hucht 2001). Niemela et al. (2008) discovered its double-lined spectroscopic (SB2) nature and presented the first orbital solution. Based on VLT/X-Shooter observations, Tramper et al. (2016) computed minimum masses of  $64.4 \pm 4.8 M_{\odot}$  and  $36.3 \pm 1.7 M_{\odot}$  for the components of the system. Additionally, they obtained their individual spectra through a disentangling method, and determined spectral types of O2.5 If\*/WN6ha for the primary (following the criteria defined by Crowther & Walborn (2011)), and O3 V((f\*))z for the secondary. The former spectral classification is congruent with the O2 If\*/WN5 presented for the star

\* E-mail: rbarba@userena.cl

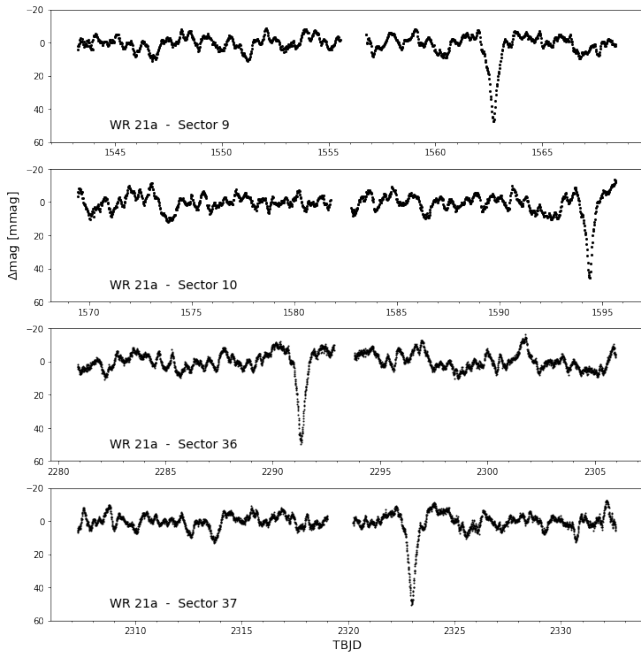


**Figure 1.** *TESS* photometric time series obtained during sectors 9, 10, 36 and 37 (from top to bottom).

in the *Galactic O Star Catalog* (Sota et al. 2014; Maíz Apellániz et al. 2016). An X-ray study by Gosset & Nazé (2016) including XMM-Newton, Chandra and Swift data showed that the emission of WR 21a in this domain exhibits small variations, except for a strengthening before periastron passage, rapidly followed by a decline as the WR star comes in front. These authors discarded eclipses as an explanation for this variability for several reasons, among them, the absence of eclipses in the UV range.

In this work we analyse for the first time the time-series of WR 21a obtained by the *TESS* mission, and combine them with existing and new radial velocity data in order to establish precise constraints on the absolute orbital parameters and, afterwards, determine the absolute stellar masses of both components.

## 2 PHOTOMETRIC DATA AND LIGHT CURVE

WR 21a was visited by the *TESS* mission in four opportunities, two in 2019 (sectors 9 and 10), and other two in 2021 (sectors 36 and 37). We have performed  $15 \times 15$  pixels cutouts (about  $315 \times 315$  arcsec) on the *TESS* Full Frame Images (FFIs) time series (Brasseur et al. 2019) centered in the position of WR 21a. The total exposure times were 1426 s for sectors 9 and 10, and 475 s for sectors 36 and 37.

We performed aperture photometry using the Python package *LIGHTKURVE* (Lightcurve Collaboration et al. 2018) version 2.09 in a Python notebook. A stellar mask of four pixels was defined interactively in order to minimize the contamination by neighbouring sources. The background mask was selected among the lowest brightness pixels in the cutouts, it includes about fifty pixels. Finally, the sky background was modelled using principal component analysis, following the package recommendations. In order to correct for low frequency variations in the time series for each sector, the extracted photometric data were normalized using a very smooth polynomial fit.

**Table 1.** Times of minima in the *TESS* photometry and *observed* minus *calculated* time of minima using the linear ephemeris of Equation 1

Sector	HJD d	Error d	( <i>O</i> – <i>C</i> ) d
09	2 458 562.7056	0.0015	0.0018
10	2 458 594.3801	0.0021	-0.0022
36	2 459 291.3130	0.0009	0.0025
37	2 459 322.9868	0.0012	-0.0022

Fig. 1 displays the resulting *TESS* light curve. It presents a clear sharp dimming of about 5 % in flux during each visit, which lasts for about 20.5 hours (0.027 in orbital phase). The overall shape resembles the light curves of the so-called *heartbeat* stars (Thompson et al. 2012). In these type of binaries, during the periastron passage, proximity effects produce a noticeable change in the brightness of the system, revealed as an electrocardiogram-style pulse, which gives rise to their denomination. The flux minima observed in WR 21a are periodically separated in time, in coincidence with the spectroscopic period, indicating that only one eclipse is detected in this system. High frequency stochastic photometric variations are also present with an amplitude of about 2 %, resembling those observed in O-type supergiants (see e.g. Burssens et al. 2020; Trigueros Páez et al. 2021). Alternatively, they could be the observational signature of tidally excited oscillations (TEO; Kumar et al. 1995; Thompson et al. 2012).

Since spectroscopic and photometric observations were obtained in different epochs between 2005 and 2021, we used the whole data set to improve the period determination and calculated a new ephemeris for the system. A direct Lomb-Scargle (Scargle 1982) periodogram analysis of the photometric data does not succeed at recovering the orbital period of 31.7-days. In subsection 4.1 we discuss in detail this periodogram. The orbital period is approximately recovered using “phase dispersion minimization” (PDM; Stellingwerf 1978), although this method does not deliver the precision needed to phase the flux minima. Therefore, we derived the photometric ephemeris directly from the measurements of the four observed times of minima, by fitting Gaussian functions to the core of each eclipse in the *TESS* time series (see Table 1). Adopting the time of minimum at sector 37 as reference epoch, the linear ephemeris for the eclipse is as follows:

$$T_{\text{ecl}}(\text{HJD}) = 2\,459\,322.989 + 31.67855\,E, \quad (1)$$

being  $E$ , the orbital cycle.

The period derived in this photometric linear ephemeris is essentially the same as for the spectroscopic orbit, confirming that the observed dimming in the light curve is related with the orbital motion.

## 3 SPECTROSCOPIC DATA AND ORBITAL SOLUTION

We calculated a new spectroscopic orbit using the RVs from Tramper et al. (2016), along with ten new RV measurements. The new epochs correspond to eight échelle spectra collected between 2005–2013 as part of the *OWN Survey* s (Barbá et al. 2017) observing campaigns (2.5-m du Pont telescope, Las Campanas Observatory, Chile), and two spectra retrieved from the ESO database (program ID 091.D-0622(A), 2.2-m ESO/MPI telescope, La Silla Observatory, Chile).

**Table 2.** Radial velocity measurements determined from the He II  $\lambda 5412$  absorption line for both components in WR 21a.

HJD d	RV <sub>prim</sub> km s <sup>-1</sup>	RV <sub>sec</sub> km s <sup>-1</sup>	instrument, telescope	R
2 453 481.536	-80		Échelle, 2.5 m, LCO	20 000
2 453 489.501	-156	229	Échelle, 2.5 m, LCO	20 000
2 453 490.540	-149	249	Échelle, 2.5 m, LCO	20 000
2 453 491.540	-187	256	Échelle, 2.5 m, LCO	20 000
2 453 772.701	-145	194	Échelle, 2.5 m, LCO	20 000
2 453 875.510	161	-288	Échelle, 2.5 m, LCO	20 000
2 454 200.583	20		Échelle, 2.5 m, LCO	20 000
2 456 435.511	-157	245	Échelle, 2.5 m, LCO	20 000
2 456 468.474	-151	231	FEROS, 2.2 m, La Silla	48 000
2 456 469.483	-152	267	FEROS, 2.2 m, La Silla	48 000

The reader is referred to Barbá et al. (2020) for details about the reduction process.

The RVs were derived through a double Gaussian fit of the He II  $\lambda 5412$  absorption line, which is clearly double in most of the spectra. To this aim, the dispersion and intensity of each Gaussian component was first determined from the analysis of the spectra in quadrature; then these parameters were kept as fixed, in order to fit only the line position. The continuum was fixed as well. Table 2 lists the heliocentric Julian days (HJD) and RVs derived for both components, together with the instrumental configuration and resolving power  $R$  of each observation.

To calculate the spectroscopic orbital solution we ran the FOTEL code (Hadrava 2004), which allows the fitting of multiple RV data sets, independently determining their systemic velocities.

The calculated systemic velocities are used as zero point corrections between the different data sets. Considering our RV measurements we obtained  $-41.5$  and  $44.0$  km s<sup>-1</sup> for the primary and secondary, respectively. The corresponding values for the RVs from Trammer et al. (2016) are  $-28.5$  and  $32.7$  km s<sup>-1</sup>. The obtained spectroscopic orbital period is  $P = 31.682 \pm 0.005$  d, which is similar to the photometric one, as we will explain below. Therefore, the spectroscopic orbital solution is determined using the FOTEL program, with the period fixed to the photometric value, and the remaining orbital parameters treated as free. The resulting orbital elements and minimum masses are shown in Table 3.

#### 4 WR 21A AS AN ECLIPSING BINARY

We modelled the *TESS* light-curve adopting the spectroscopic orbital solution previously determined, using the PHysics Of Eclipsing BinariEs (PHOEBE) package version 2.3 (Prša & Zwitter 2005; Prša et al. 2016). Technical details and computational procedures are described in Prša (2018).

We adopted the photometric ephemeris of equation 1 and performed the analysis of the system using PHOEBE. To calculate a binary model, some input parameters are required. Both stellar components in WR 21a are very hot massive stars. We have constrained the effective temperature ( $T_{\text{eff}}$ ) of the O2.5 If\*/WN6ha and O3 V((f\*))z components to 42 000 K, and 48 000 K, respectively. For the O2.5 If\*/WN6ha component we adopted the  $T_{\text{eff}}$  used by Bonanos et al. (2004) for the O3 If\*/WN6 components of WR 20a, which are spectroscopically very similar to WR 21a. For the O3 V star, we adopted a  $T_{\text{eff}}$  slightly larger than the O3-3.5 V component of HD 150136 ( $46\,500 \pm 1000$  K; Mahy et al. 2018), and similar to the  $T_{\text{eff}}$  calculated from model atmospheres by Martins &

**Table 3.** Orbital solution and stellar parameters.

Parameters obtained from the <i>TESS</i> light curve		
$P$ [d]	$31.67855 \pm 0.00002$	
$T_{\text{ecl}}$ [HJD]	$2\,459\,322.989 \pm 0.001$	
Orbital parameters obtained through the <i>FOTEL</i> code		
Parameter	Primary	Secondary
$T_{\text{periastron}}$ [HJD]	$2\,459\,323.144 \pm 0.001$	
$e$	$0.695 \pm 0.007$	
$\omega$ [°]	$286.8 \pm 1.0$	
$K_i$ [km s <sup>−1</sup> ]	$158.0 \pm 2.7$	$278.1 \pm 2.8$
$a_i \sin i$ [R <sub>⊙</sub> ]	71.1	125.2
$M_i \sin^3 i$ [M <sub>⊙</sub> ]	64.6	36.7
$q$ [M <sub>2</sub> /M <sub>1</sub> ]	$0.568 \pm 0.011$	
r.m.s <sub>(O−C)</sub> [km s <sup>−1</sup> ]	9.7	10.8
Stellar parameters obtained by means the <i>PHOEBE</i> code		
$i$ [°]	$61.8 \pm 1.5$	
$T_{\text{eff}}$ [K]	42 000 (fixed)	48 000 (fixed)
$M_i$ [M <sub>⊙</sub> ]	94.4	53.6
$R_i$ [R <sub>⊙</sub> ]	$23.3 \pm 1.6$	$14.8 \pm 2.0$
$\log g_i$	3.69	3.81
$\log L$ [L <sub>⊙</sub> ]	$6.18 \pm 0.06$	$6.02 \pm 0.09$
$M_{\text{bol}}$ [mag]	$-10.71 \pm 0.15$	$-10.30 \pm 0.22$

Palacios (2017) for the spectral type O3 V ( $T_{\text{eff}} = 48\,000$  K). The  $T_{\text{eff}}$  of both components in the system are outside the supported ATLAS-9 grid model atmospheres (Castelli & Kurucz 2003), hence, we used the PHOEBE option *blackbody* to model the atmospheres, along with the *TESS* passband. We assumed the *logarithmic law* to describe the limb-darkening model, using the coefficients calculated by Claret (2000) and Claret (2017) for the bolometric and passband limb-darkening, respectively. We should mention that the adopted limb-darkening components correspond to models for  $T_{\text{eff}} = 40\,000$  K and  $\log g = 4.0$ , because the calculated values for hotter models are suitable for sub-dwarf stars ( $\log g > 4.5$ ), but not for massive stars. We also assume a bolometric albedo equal to 1 for both stars. Orbital geometry (projected semi-axes,  $a_{12} \sin i$ ; argument of periastron,  $\omega$ ), and mass ratio ( $q = M_{\text{O3}}/M_{\text{O2.5/WN6}}$ ) are fixed from the spectroscopic orbital solution.

As the *TESS* light-curve reveals only one eclipse, it is not possible to obtain absolute values for the star radii without additional constraints on the radius of at least one component. Absolute radius of VMS are roughly determined for a few systems, as the case of the massive twin eclipsing system WR 20a, O3 If\*/WN6 + O3 If\*/WN6 (Bonanos et al. 2004; Rauw et al. 2004). This system is composed of stars with spectroscopic classification similar to WR 21a, but their binary configuration is near *contact*, i.e. both stars are very distorted, almost filling their Roche lobes, which is not the case for WR 21a. Thus, we adopted as a starting point  $R_1 = 20 R_{\odot}$ , as a representative radius of the O2.5/WN6 component.

With these assumptions, we computed different models just changing the orbital inclination from  $90^\circ$  towards lower values, following a coarse step of  $2^\circ$ . The first obvious conclusion is that at high inclinations ( $i \sim 90^\circ$ ) models produce two deep eclipses. With  $i \sim 84^\circ$ , models start to show only one eclipse, being the O star eclipsed by the O2.5/WN6 component. At these inclinations, the observed eclipse depth would only be achieved with a radius of the O-type

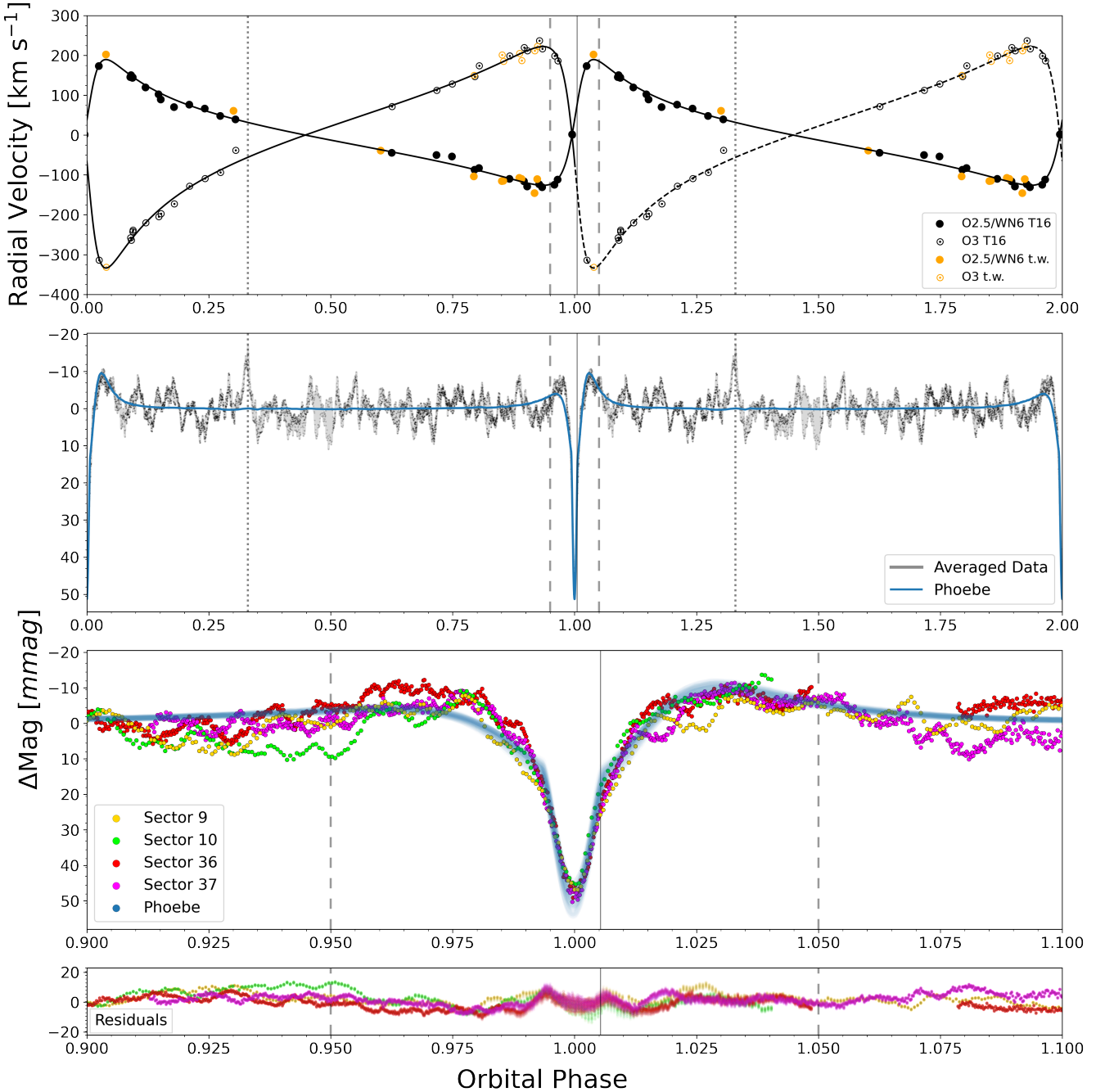


**Figure 2.** Top: RV curves of the WN and O components using the values of [Tramper et al. \(2016\)](#) and Table 2 (corrected by their respective systemic velocities); Middle-top: Averaged *TESS* light curve and the adopted *PHOEBE* model. Middle-bottom: Comparison between the best 50 *PHOEBE* models (in light blue) with the photometric time series observed in the four sectors (plotted with different colours for a better visualisation). Light curves are zoomed in the orbital phases considered in the statistical analysis of r.m.s. (i.e.  $\phi=0.95$  and  $1.05$ ). Bottom: residuals derived from *TESS* photometric observations and *PHOEBE* models.

star  $R_2 = 4.5 R_\odot$ , which is much smaller than what is expected ( $R_{O3} = 13.8 R_\odot$ , c.f., [Martins et al. 2005](#)). Models improve around  $i \sim 65^\circ$ , when the secondary radius gets  $R_2 \sim 11 R_\odot$ .

Therefore, we have calculated  $21 \times 11 \times 11 = 2541$  models in the range of  $i = [55^\circ, 65^\circ]$ , at steps of  $\Delta i = 0.5^\circ$ , and stellar radii in the ranges of  $R_1 = [20, 30] R_\odot$ , and  $R_2 = [11, 21] R_\odot$ , with steps of  $\Delta R_{1,2} = 1 R_\odot$ . Fig. 2 (mid-top panel) shows the best model fitted to the averaged light-curve. We calculated the root-mean-squared

(r.m.s.) from the model and the observed light-curve only in the orbital phases centred in the eclipse, in the interval  $\Delta\phi = [-0.05, 0.05]$  (a tenth of the orbital period). The remaining orbital phases were also modelled, but they are not used for the r.m.s. computation because the light curve is dominated by oscillations and the model is constant in flux. The eclipses observed in each of the four *TESS* sectors are differently affected by such photometric variations, producing subtle changes in the depth and width.



The eclipse is zoomed in the mid-bottom panel of Fig. 2, depicting the photometric time series for the four *TESS* sectors. Superimposed are the best 50 *PHOEBE* models. Their residuals are presented in the bottom panel.

Overall, the *PHOEBE* models describe fairly well the observations. The asymmetric shape reminiscent of the *heartbeat* stars is recovered, although some features should be highlighted. In the case of WR 21a, the periastron passage is at orbital phase  $\phi = 0.0049$ , i.e. during the eclipse of the O3 star (dotted line in Fig. 2), hence any manifestation of the *heartbeat* effect must be observed close to those phases (i.e. eclipse). The shape of the eclipse core is satisfactorily modelled. The eclipse egress is fairly modelled, too, including the characteristic *heartbeat* bump after the periastron passage (see Fig. 3), which can be explained in part as mutual irradiation effects. The computed models show a small flux excess (2 mmag) in orbital phases before the eclipse, signature of the *heartbeat* effect, but a small (5 mmag) systematic deviation from observations is still present in some orbital cycles, noticeable in sector 36 during orbital phases  $\phi = [0.975 - 0.990]$ . Another interesting feature is the bump with an amplitude of about 15 mmag located at the inferior conjunction ( $\phi = 0.33$ ). At this orbital phase, the stars are very well separated,  $346 R_{\odot}$  (c.f. Fig. 3, bottom panel), then the bump does not arise from the mutual irradiation of the stars.

The upper-left panel of Fig. 4 shows the 3-D r.m.s. distribution of the observed and computed light-curves for the interval of selected parameters ( $i$ ,  $R_1$ ,  $R_2$ ). The remaining panels represent cuts in different planes, ( $R_1$ ,  $R_2$ ), ( $R_1$ ,  $i$ ), and ( $R_2$ ,  $i$ ), at the position of the best solution. It is necessary to note the model dependence, for a given inclination, with radius of the secondary component in function of the adopted radius for the primary component: smaller radii for the primary imply larger radii for the secondary, and vice versa (see r.m.s.  $R_1$  vs  $R_2$  panel in Fig. 4).

The final parameters obtained for  $i$ ,  $R_1$  and  $R_2$  are derived from the average of the best 50 models, and they are shown in Table 3, where the listed errors correspond to standard deviations.

#### 4.1 Tidally excited oscillations

Fig. 1 shows that the *TESS* light-curve of WR 21a is ridden by a pattern of irregular variations with an amplitude up to 20 mmag. In order to characterise these low-amplitude and high-frequency variations we removed the eclipse feature from the light-curve, and then we calculated a periodogram. Interestingly, the most significant frequencies show certain coupling with the orbital period (eleven are listed in Table 4, where the last column shows the ratio between pulsational and orbital frequencies). WR 21a is a system composed by two very massive stars in a highly eccentric orbit, then, we could expect that strong time-dependent tidal forces may induce pulsations, a mechanism known as tidally excited oscillations (TEOs) (Kumar et al. 1995).

As pointed out by Kołaczek-Szymański et al. (2021), TEOs can be recognized in the frequency spectrum of the light curve as harmonics of the orbital frequency. As we show in Table 4, the most significant frequencies are  $n$ -times the orbital frequency, being the orbital harmonics  $n = 5, 7, 9, 14, 17, 18, 25, 27, 33, 54$ , that means all these frequencies could be related to TEOs. Kołaczek-Szymański et al. (2021) proposed that the massive WN+WN+O multiple system HD 5980 in the Small Magellanic Cloud (Koenigsberger et al. 2014) is the most massive star known with a *heartbeat* effect, and probably with TEOs (Hillier et al. 2019) with a frequency of  $3.96 \text{ d}^{-1}$ . The present analysis shows that WR 21a is one of the most massive systems known to present TEOs and a *heartbeat* system as well.

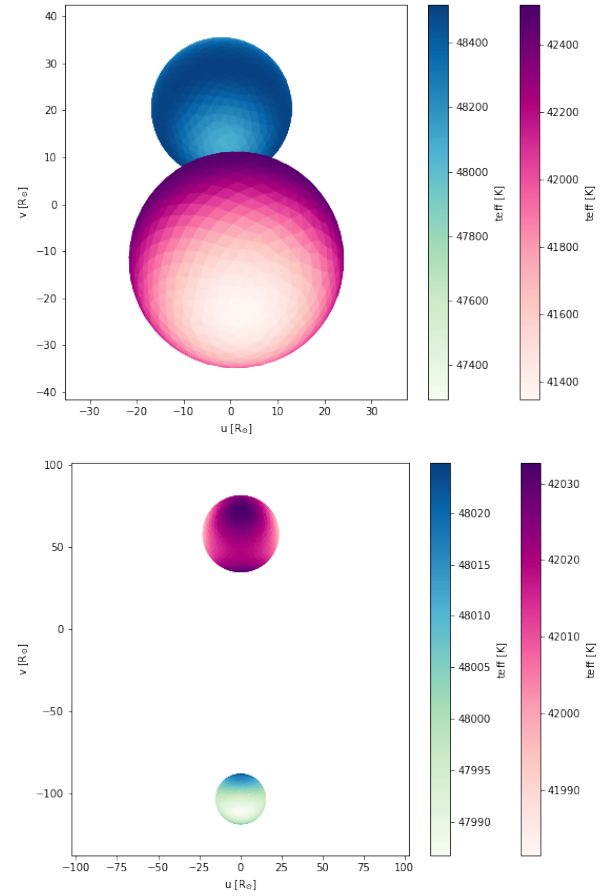


**Figure 3.** Geometric model of WR 21a in the eclipse (top panel), and in the inferior conjunction (bottom panel), as seen in the plane of the sky. Note the change in the  $T_{\text{eff}}$  of the stars during the eclipse (near periastron passage). Interestingly, the tidal deformation of the O2.5/WN6 (in magenta) during that moment produces a  $T_{\text{eff}}$  drop of more than 600 K in the back side of the star. Conversely, the O3-component (in blue) is somewhat cooler in the bulge facing the primary component but hotter in the surrounding areas. During the inferior conjunction, the  $T_{\text{eff}}$  of the stars is very homogeneous ( $\Delta T_{\text{eff}} < 70 \text{ K}$ ). The colour maps are centred in the  $T_{\text{eff}}$  adopted for each star.

This fact is further supported by the computation of the normalised tidal potential energy,  $\bar{\epsilon}$  (see eq. 6 in Kołaczek-Szymański et al. 2021), which is an indication of the amount of tidal deformation in the binary components. This parameter is related to the ratio of tidal potential energy concentrated in tidal bulges at the periastron versus the gravitational binding energy of both components. The value of  $\bar{\epsilon}$  computed for WR 21a is  $\log \bar{\epsilon} = -6.7$ , while it is  $-7.3$  for HD 5980. Thus, with a total mass of  $148 M_{\odot}$  ( $\log M_1 + M_2 = 2.17$ ), WR 21a is located to the right and above of the position of HD 5980 in Kołaczek-Szymański et al. (2021), Figure 15.

#### 5 CONCLUDING REMARKS

We unveiled four eclipses in the very massive binary system WR 21a using photometric time series collected by the *TESS* mission. The overall shape of the light curve during the eclipse phases mimics that of *heartbeat* systems. We fitted binary models to the light-curve by means of the *PHOEBE* code. Models were built based on a grid of radii for both massive components, and inclinations, keeping fixed the

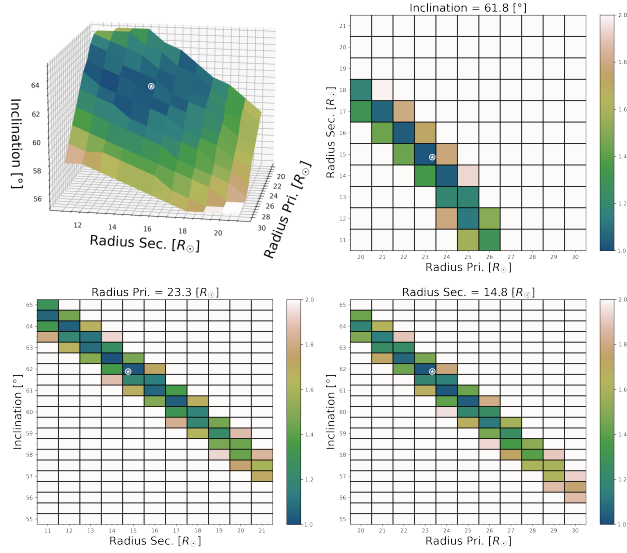


**Figure 4.** 3-D map distribution of normalised r.m.s. values for the set of parameters ( $i$ ,  $R_1$ ,  $R_2$ ) used to calculate the PHOEBE models (upper-left). The other three panels show orthogonal cuts at the position of the adopted averaged values for  $R_1$ ,  $R_2$  and  $i$ : ( $R_1$ ,  $R_2$ ) at fixed  $i$  (upper-right), ( $R_2$ ,  $i$ ) at fixed  $R_1$  (lower-left), and ( $R_1$ ,  $i$ ) at fixed  $R_2$  (lower-right). The colour bar represents normalised r.m.s. values.

**Table 4.** The eleven most significant frequencies in *TESS* photometric time series of WR 21a.

#	Frequency $\text{d}^{-1}$	Period $\text{d}$	Power	$f_n/f_{\text{orbit}}$
1	0.22069	4.53118	310	7.0
2	0.43909	2.27744	255	13.9
3	0.15687	6.37487	226	5.0
4	1.71025	0.58471	218	54.2
5	0.85512	1.16943	149	27.1
6	0.79052	1.26499	137	25.0
7	0.52829	1.89289	125	16.7
8	0.28837	3.46783	91	9.1
9	1.04199	0.95971	69	33.0
10	0.27991	3.57263	68	8.9
11	0.56828	1.75969	65	18.0

spectroscopic orbital elements and mass ratio. We have determined the best set of model parameters,  $R_1$ ,  $R_2$  and  $i$ , through a r.m.s. minimization method, and the dependence between them (see Fig. 4) allow us to estimate a validity interval. The orbital inclination,  $i = 61.8 \pm 1.5^\circ$  is the key parameter to calculate the absolute stellar masses of the system.

The massive O3 V((f\*))z companion is characterised as a star with an absolute mass of  $M_2 = 53.6 M_\odot$ , and a radius of  $14.8 R_\odot$ . There are only two Galactic O3-type stars for which absolute mass determinations are available; those are the O3.5 V components of the triple system HD 150136 and the O3.5 V primary component of the SB2 system HD 93205. For HD 150136, Sana et al. (2013), using the PIONIER combiner at the Very Large Telescope Interferometer (VLTI), derived the three-dimensional orbit of the outer system, which combined with the RV curves of the inner pair, allowed to calculate a mass of  $62.6 \pm 10 M_\odot$  for the O3.5 component. In the case of HD 93205, a high-quality spectroscopic solution was determined

by Morrell et al. (2001), which was used to derive absolute masses based on apsidal motion analysis (Benvenuto et al. 2002). The mass determined for the O3.5 component is  $60 \pm 19 M_\odot$ . Therefore, our empirical mass determination for the O3-component in WR 21a is comfortably located in the mass range of similar stars in massive systems.

We have obtained a mass of  $94.4 \pm 5 M_\odot$  for the O2.5 If\*/WN6ha component, confirming it as a VMS. We must remark that reliable dynamical masses of Galactic VMS, i.e. determined through the spectroscopic and photometric calculation of orbital parameters in eclipsing systems, are very scarce. Among the Galactic systems, we bring up NGC 3603-A1 ( $116+89 M_\odot$ ; Schnurr et al. 2008), WR 20a ( $82+83 M_\odot$ ; Bonanos et al. 2004), and Arches F2 (WR 102aa,  $82+60 M_\odot$ ; Lohr et al. 2018). These three massive systems present light curves compatible with near-contact eclipsing SB2 binaries, in contrast to the case of WR 21a, which is clearly a detached system. The radius of the O2.5 If\*/WN6ha component is slightly larger than that measured for the components of the eclipsing system WR 20a. If WR 21a was ejected from the massive star cluster Westerlund 2 as proposed (Roman-Lopes et al. 2011), both WR 21a and WR 20a should have the same age, and thus the radius difference would be related to the mass difference, being the former more massive.

This discovery places WR 21a as a new benchmark for the evolutionary analysis of VMS. Its light curve indicates that both components are well detached, which is also confirmed by the computed star radii. Given the youth of these stars, they are still evolving independently, before the first mass-transfer stage. The presence of tidally excited oscillations opens the possibility of studying in detail the relationship of tidal oscillations and internal structure of the stars.

## ACKNOWLEDGEMENTS

RHB acknowledges support from ANID FONDECYT Regular Project No. 1211903. RG acknowledges support from grant PICT 2019-0344. Also, we thank the director and staff at LCO for the use of their facilities and kind hospitality during the observing runs. RHB, RG and NM thank to Diego Armando Maradona (Barrilete Cósmico), for brightening up our lives.

Software. This research made use of Lightcurve, a Python package for Kepler and *TESS* data analysis (Lightcurve Collaboration, 2018) (<https://docs.lightcurve.org/index.html>), and "PHysics Of Eclipsing BinariEs" (PHOEBE) package (<http://phoebe-project.org>).

## DATA AVAILABILITY

This paper is based on public data of the *TESS* mission, and spectroscopic data belonging to the *OWN Survey* team, available on reasonable request to Dr. Rodolfo H. Barbá, the public ESO database, and published radial velocities (Tramper et al. 2016).

## REFERENCES

- Barbá R. H., Gamen R., Arias J. I., Morrell N. I., 2017, in Eldridge J. J., Bray J. C., McClelland L. A. S., Xiao L., eds, IAU Symposium Vol. 329, The Lives and Death-Throes of Massive Stars. pp 89–96, doi:10.1017/S1743921317003258
- Barbá R. H., et al., 2020, *MNRAS*, **494**, 3937

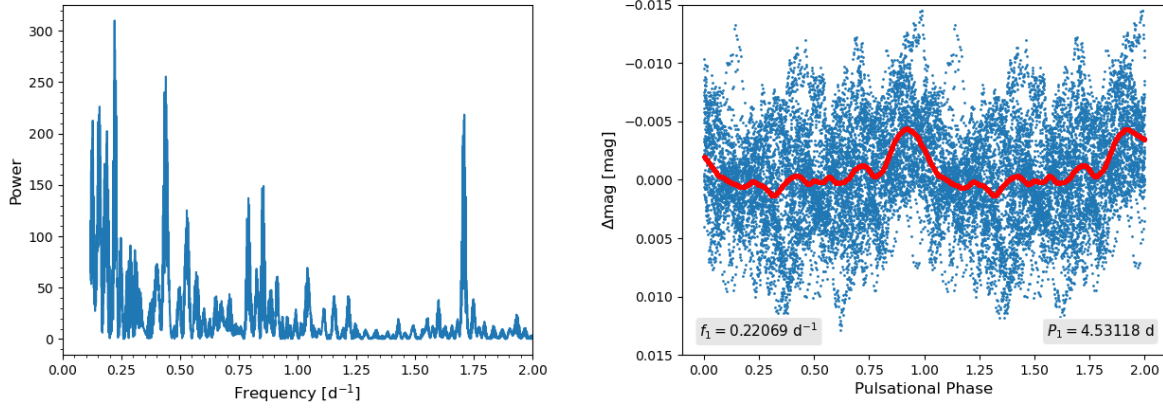


**Figure 5.** Left: Lomb-Scargle periodogram of *eclipse cleaned* TESS light curve of WR 21a. Right: phased light-curve using the first frequency,  $f_1 = 0.22069 \text{ d}^{-1}$ . The red line is a smoothing to the folded light curve

Benvenuto O. G., Serenelli A. M., Althaus L. G., Barbá R. H., Morrell N. I., 2002, *MNRAS*, **330**, 435

Bestenlehner J. M., et al., 2020, *MNRAS*, **499**, 1918

Bonanos A. Z., et al., 2004, *ApJ*, **611**, L33

Brasseur C. E., Phillip C., Fleming S. W., Mullally S. E., White R. L., 2019, *Astrotcut: Tools for creating cutouts of TESS images* (ascl:1905.007)

Burssens S., et al., 2020, *A&A*, **639**, A81

Caraveo P. A., Bignami G. F., Goldwurm A., 1989, *ApJ*, **338**, 338

Castelli F., Kurucz R. L., 2003, in Piskunov N., Weiss W. W., Gray D. F., eds, Vol. 210, *Modelling of Stellar Atmospheres*. p. A20 ([arXiv:astro-ph/0405087](https://arxiv.org/abs/astro-ph/0405087))

Claret A., 2000, *A&A*, **363**, 1081

Claret A., 2017, *A&A*, **600**, A30

Crowther P. A., Walborn N. R., 2011, *MNRAS*, **416**, 1311

Crowther P. A., Schnurr O., Hirschi R., Yusof N., Parker R. J., Goodwin S. P., Kassim H. A., 2010, *MNRAS*, **408**, 731

Gosset E., Nazé Y., 2016, *A&A*, **590**, A113

Hadrava P., 2004, *Publications of the Astronomical Institute of the Czechoslovak Academy of Sciences*, **92**, 1

Hillier D. J., Koenigsberger G., Nazé Y., Morrell N., Barbá R. H., Gamen R., 2019, *MNRAS*, **486**, 725

Koenigsberger G., Morrell N., Hillier D. J., Gamen R., Schneider F. R. N., González-Jiménez N., Langer N., Barbá R., 2014, *AJ*, **148**, 62

Kołaczek-Szymański P. A., Pigulski A., Michalska G., Moździerski D., Różański T., 2021, *A&A*, **647**, A12

Kumar P., Ao C. O., Quataert E. J., 1995, *ApJ*, **449**, 294

Langer N., 2012, *ARA&A*, **50**, 107

Lightcurve Collaboration et al., 2018, *Lightcurve: Kepler and TESS time series analysis in Python*, *Astrophysics Source Code Library* (ascl:1812.013)

Lohr M. E., Clark J. S., Najarro F., Patrick L. R., Crowther P. A., Evans C. J., 2018, *A&A*, **617**, A66

Mahy L., et al., 2018, *A&A*, **616**, A75

Maíz Apellániz J., et al., 2016, *ApJS*, **224**, 4

Martins F., Palacios A., 2017, *A&A*, **598**, A56

Martins F., Schaerer D., Hillier D. J., 2005, *A&A*, **436**, 1049

Mereghetti S., Belloni T., Shara M., Drissen L., 1994, *ApJ*, **424**, 943

Morrell N. I., et al., 2001, *MNRAS*, **326**, 85

Niemela V. S., Gamen R. C., Barbá R. H., Fernández Lajús E., Benaglia P., Solivella G. R., Reig P., Coe M. J., 2008, *MNRAS*, **389**, 1447

Prša A., Zwitter T., 2005, *ApJ*, **628**, 426

Prša A., 2018, *Modeling and Analysis of Eclipsing Binary Stars: The theory and design principles of PHOEBE*, [doi:10.1088/978-0-7503-1287-5](https://doi.org/10.1088/978-0-7503-1287-5).

Prša A., et al., 2016, *ApJS*, **227**, 29

Rauw G., et al., 2004, *A&A*, **420**, L9

Ricker G. R., et al., 2015, *Journal of Astronomical Telescopes, Instruments,*

*and Systems*, **1**, 014003

Roman-Lopes A., Barba R. H., Morrell N. I., 2011, *MNRAS*, **416**, 501

Sana H., 2017, in Eldridge J. J., Bray J. C., McClelland L. A. S., Xiao L., eds, *IAU Symposium Vol. 329, The Lives and Death-Throes of Massive Stars*. pp 110–117 ([arXiv:1703.01608](https://arxiv.org/abs/1703.01608)), [doi:10.1017/S1743921317003209](https://doi.org/10.1017/S1743921317003209)

Sana H., et al., 2012, *Science*, **337**, 444

Sana H., Le Bouquin J. B., Mahy L., Absil O., De Becker M., Gosset E., 2013, *A&A*, **553**, A131

Scargle J. D., 1982, *ApJ*, **263**, 835

Schnurr O., Casoli J., Chené A. N., Moffat A. F. J., St-Louis N., 2008, *MNRAS*, **389**, L38

Sota A., Maíz Apellániz J., Morrell N. I., Barbá R. H., Walborn N. R., Gamen R. C., Arias J. I., Alfaro E. J., 2014, *ApJS*, **211**, 10

Stellingwerf R. F., 1978, *ApJ*, **224**, 953

The P. S., 1966, *Contributions from the Bosscha Observatory*, **35**, 1

Thompson S. E., et al., 2012, *ApJ*, **753**, 86

Tramper F., Sana H., Fitzsimons N. E., de Koter A., Kaper L., Mahy L., Moffat A., 2016, *MNRAS*, **455**, 1275

Trigueros Páez E., Barbá R. H., Negueruela I., Maíz Apellániz J., Simón-Díaz S., Holgado G., 2021, *arXiv e-prints*, [p. arXiv:2106.08865](https://arxiv.org/abs/2106.08865)

Vink J. S., 2015, *Very Massive Stars in the Local Universe*. Vol. 412, [doi:10.1007/978-3-319-09596-7](https://doi.org/10.1007/978-3-319-09596-7).

Wackerling L. R., 1970, *Mem. RAS*, **73**, 153

van der Hucht K. A., 2001, *New Astronomy Review*, **45**, 135

This paper has been typeset from a  $\text{\LaTeX}$  file prepared by the author.